ACS APPLIED MATERIALS & INTERFACES

Research Article

Cite This: ACS Appl. Mater. Interfaces 2019, 11, 48551−48555

www.acsami.org

Manipulating Charge Transfer from Core to Shell in CdSe/CdS/Au Heterojunction Quantum Dots

Exian Liu,[†,‡] Hua Zhu,[§] Jun Yi,[†,‡] Kanishka Kobbekaduwa,[‡] Pan Adhikari,[‡] Jianjun Liu,[†] Ying Shi,[∥] Jianbing Zhang,[⊥] Hongbo Li,[#] Ana Oprisan,[▽] Apparao M. Rao,[‡] Hugo Sanabria,[*,‡] Ou Chen,[*,§] and Jianbo Gao[*,‡]

[†]Key Laboratory for Micro/Nano Optoelectronic Devices of Ministry of Education, Hunan Provincial Key Laboratory of Low-Dimensional Structural Physics and Devices, School of Physics and Electronics, Hunan University, Changsha 410082, China

[‡]Department of Physics and Astronomy, Ultrafast Photophysics of Quantum Devices Laboratory, Clemson University, Clemson, South Carolina 29634, United States

[§]Department of Chemistry, Brown University, Providence, Rhode Island 02912, United States

[∥]Institute of Atomic and Molecular Physics, Jilin Provincial Key Laboratory of Applied Atomic and Molecular Spectroscopy, Jilin University, Changchun 130012, China

[⊥]School of Optical and Electronic Information, Huazhong University of Science and Technology, Wuhan 430074, China

[#]School of Materials Science and Engineering, Beijing Institute of Technology, Beijing 100081, China

[▽]Department of Physics and Astronomy, College of Charleston, Charleston, South Carolina 29401, United States

Supporting Information

ABSTRACT: The photophysics of charge-transfer and recombination mechanisms in a heterojunction structure of CdSe/CdS/Au quantum dots (QDs) are studied by temperature-dependent steady-state photoluminescence (PL) and time-resolved PL (TRPL). We manipulate the charge transfer from core to shell surface by varying the tunneling barrier height resulting from temperature variation and the barrier width resulting from shell thickness variation. The charge-transfer process, which can be described by a tunneling transmission model, is manifested by two competitive recombination processes, an intrinsic exciton emission and a trap emission in the near-infrared (NIR) range. Our study establishes the photophysics foundation for the core/shell/metal application in photocatalyst and optoelectronics.

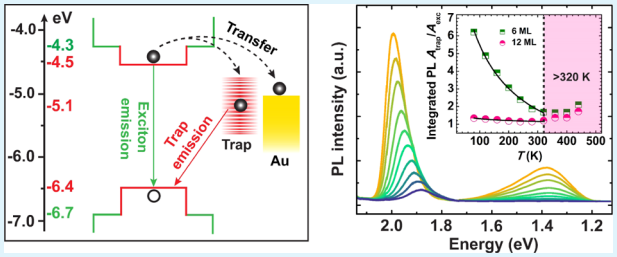

KEYWORDS: *time resolved, steady state, photoluminescence, core/shell, tunneling, recombination*

1. INTRODUCTION

Quantum dots or nanorods decorated with metal nanoparticles such as gold (Au) and platinum (Pt) have considerable applications in photocatalysis[1−9] and optoelectronics[10−12] due to their novel properties such as high surface-to-volume ratio, hot carrier, and carrier multiplication.[13−16] Therefore, understanding the fundamental photophysics mechanisms including charge-transfer and recombination processes in these systems is the foundation to tune their optical and electrical functionalities. Very often, to reduce surface defect states and Auger recombination process, the core quantum dots are passivated with a shell to form a core/shell heterojunction structure.[17−19] As a result, the shell quality plays a significant role in tuning charge-transfer and recombination processes.[20,21] However, the study of influence of shell, which addresses the interplay between intrinsic excitons and shell-related surface states in trap-related core/shell/metal quantum dot (QD) is currently lacking. This is due to the hard-detected or very weak surface state emission originating from the strong quenching of metal domain on intrinsic emission in these systems.[1,22] In addition to the shell property, the charge carrier recombination and transfer from core to shell surface also depend on the band offset between the core and shell that relies on temperature parameter. However, in surface state-related core/shell/metal QDs system, how do these two competing mechanisms vary with temperature still remains unclear.

In this report, to comprehensively understand the interplay between charge-transfer and recombination mechanisms in CdSe/CdS/Au heterojunction nanocrystals, we study these systems with temperature-dependent steady-state photoluminescence (PL) and time-resolved PL (TRPL). We manipulate the charge transfer to shell surface by varying the tunneling barrier height resulting from temperature variation and the

Received: September 24, 2019
Accepted: November 29, 2019
Published: November 29, 2019

DOI: 10.1021/acsami.9b17339
ACS Appl. Mater. Interfaces 2019, 11, 48551−48555

barrier width resulting from shell thickness variation. These mechanisms are manifested by an intrinsic exciton emission and trap emission in the near-infrared (NIR) range. These two competitive recombination processes can be described by a tunneling transmission model.

2. RESULTS AND DISCUSSION

2.1. Temperature-Dependent Steady-State PL. Four samples are synthesized with two different shell thickness (~6 and 12 MLs) using the synthesis procedure from our previous work[2] (see Experimental Section and the Supporting Information), and detailed parameters are listed in Table 1.

Table 1. Detailed Parameters of Two Shell Thickness Structures of CdSe/CdS and CdSe/CdS/Au QDs[a]

	shell (ML)	d_{core} (nm)	T_{shell} (nm)	E_g (eV)	E_{trap} (eV)
QD	6	4.2	2.6	1.911	
	12	4.2	5.4	1.876	
QD−Au	6	4.2	2.6	1.938	1.351
	12	4.2	5.4	1.925	1.392

[a]These parameters include the core diameter (d_{core}), the shell thickness (T_{shell}), the intrinsic band gap (E_g), and the surface state (trap state) related peak energy (E_{trap}) for QD−Au at room temperature. The diameter of Au nanoparticle is 2 nm.

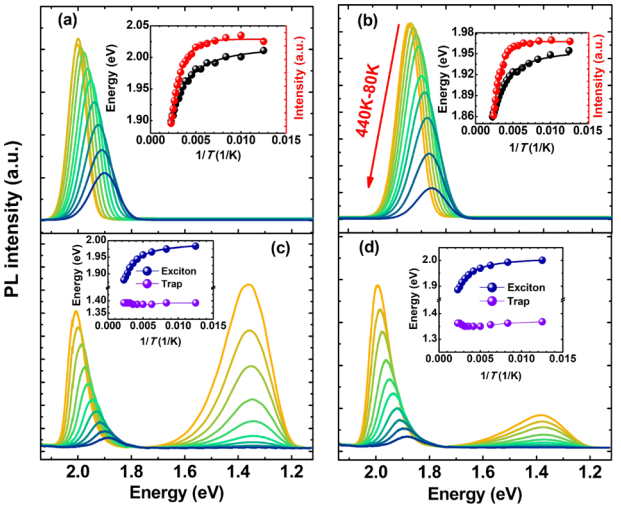

Figure 2. Normalized temperature-dependent emission for 6-ML shell CdSe/CdS (a), 12-ML shell CdSe/CdS (b), 6-ML shell CdSe/CdS/Au (c), and 12-ML shell CdSe/CdS/Au (d) in the temperature range from 80 to 440 K with a step size of 40 K. Insets (a) and (b) show the temperature dependence of PL peak energy and intensity. Insets (c) and (d) show the temperature dependence of PL peak energy for excitonic emission and trap emission. All of the PL spectra are taken at the excitation wavelength of 560 nm.

Preparation of core/shell-only CdSe/CdS QDs can be seen as an excellent photophysics comparison with Au-decorated system to clearly examine the existence of surface traps. Absorption and emission spectra of CdSe/CdS QDs show the only main intrinsic exciton emission with narrow PL peaks (Figure S1). On the other hand, once Au nanoparticles grow on the shell surface, as demonstrated by Figure 1a and insets [transmission electron microscopy (TEM) images] of Figure 1b,c, there appears a broad NIR emission for both shell thickness dots, in addition to the main intrinsic exciton emission. However, the NIR emission becomes weak with increase in shell thickness, while the PL peak shifts slightly on a scale of <50 meV as demonstrated in Figure 1c. The main exciton emission still keeps narrow PL full width at half-maximum (FWHM), which indicates that the core CdSe remains almost unaffected by the formation of QD−Au heterojunction.

To address the nature of the NIR emission, the temperature-dependent steady-state PL is demonstrated in Figure 2. First, it can be clearly seen that CdSe/CdS/Au QD films emit NIR wavelength light, while the feature of this NIR emission is not demonstrated in the CdSe/CdS core/shell QDs despite variable temperature. Thus, the NIR emission does not arise from the core/shell interfacial trap states due to the well passivation. Second, we preclude the possibility of metal-related transfer-recombination process where electron can initially transfer to Au particles and then go back to the core to recombine with the holes because the separated states have a long lifetime on a scale of microsecond or hundreds of nanoseconds for charge annihilation with no emission.[23,24] Third, the NIR emission energy is independent of the material of metal particles, while same wavelength emission is also observed in the CdSe/CdS/Pt heterojunction structure (Figure S2). Therefore, we conclude that the NIR emission is attributed to the radiative surface states or trap states on the shell surface that are formed during the growth of metal (see Experimental Section). In addition, the existence of metal on the shell surface can potentially drive the photogenerated electron transfer to the shell surface through shell thickness,[22] facilitating trap emission occurrence.

For the CdSe/CdSe core/shell structure, the behaviors of peak energy, PL intensity, and FWHM dependence on temperature are well understood by the interaction between exciton and phonon.[25−27] In general, as Figure 2a,b indicates,

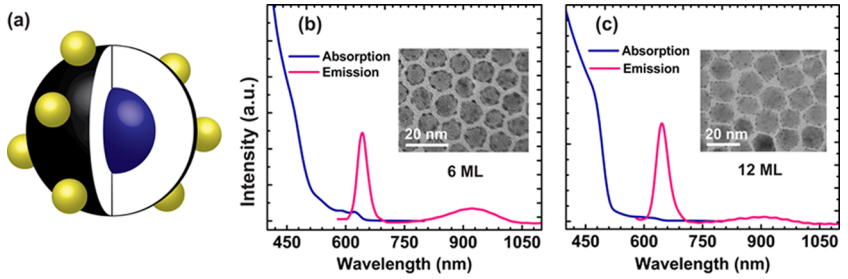

Figure 1. (a) Schematic core/shell/Au heterojunction structure. (b) Absorption and emission spectra of CdSe/CdS/Au with 6-monolayer (ML) shell (b) and 12-ML shell (c) in hexane solution. The emission spectra are normalized at 560 nm excitation wavelength. The insets show the corresponding transmission electron microscopy (TEM) images with scale bar of 20 nm.

DOI: 10.1021/acsami.9b17339
ACS Appl. Mater. Interfaces 2019, 11, 48551−48555

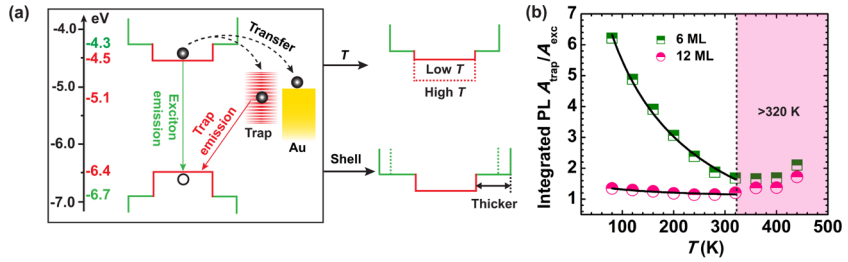

Figure 3. (a) Schematic band diagram of core/shell/Au heterojunction structure at room temperature. The right panel indicates the band diagram shift due to the variation of temperature and thickness. (b) The dependence of area ratio (A_{trap}/A_{exc}) of integrated PL emission with temperature. The solid lines are the fitting curve according to eq 1.

the peak energy decreases with increase in temperature, reflecting a reduction of energy band gap, which is due to the effect of exciton−phonon coupling and lattice deformation potential.[26] Change in peak energy can match the empirical Varshni relation[28] (eq S1, Table S1). Decrease in PL intensity with increase in temperature results from the enhancement of the nonradiative recombination such as surface carrier trapping and multiple longitudinal-optical phonon-assisted thermal escape from dots.[29,30] The thermal activation energy can be extracted by an Arrhenius relation from the PL intensity dependence on temperature (eq S2, Table S2).[31]

In contrast to core/shell only, the heterojunction structure of core/shell/Au QDs demonstrates more characteristics due to different recombination mechanisms, as illustrated in Figure 2c,d. At low temperature, trap emission peak for the 6-ML shell system has a stronger intensity than that of the main exciton emission, indicating more photogenerated electrons can tunnel from core to shell surface for the radiative trap recombination. On the other hand, the peak intensity decreases as the shell thickness is increased to 12 MLs, suggesting a stronger electron diminution with a longer tunneling distance. As the temperature further increases, the trap peak intensity decreases faster than the excitonic emission and eventually vanishes despite shell thickness at the temperature of 400 K. Therefore, this highly suggests that the trap emission intensity and electron tunneling probability strongly depend on the temperature and shell thickness. As demonstrated in the insets in Figure 2c,d, the main exciton emission peak for 6- and 12-ML structures have a similar dependence on temperature in the core/shell-only system, while the trap emission peak wavelength is almost temperature independent. This indicates that the trap energy levels shift along with the conduction band or the valence band. In particular, over the temperature range, the maximum shift of the trap emission peak is ∼6.1 meV (∼18.0 meV) for the 6-ML shell system (12-ML shell system), significantly smaller than that of the exciton emission ∼111.97 meV (∼ 94.69 meV) for the 6-ML shell system (12-ML shell system), as shown by the insets in Figure 2c,d. We attribute the high intensity of trap emission at low temperature to the reduced core/shell interface band offset that leads to a higher electron tunneling probability. The decreased intensity for a thicker-shell CdSe/CdS/Au is because of the reduced electron−hole overlapping. In addition, the shell thickness and temperature dependence of FWHM is also calculated for two systems, suggesting that a thicker (12 MLs) shell and a higher temperature can result in more broadened FWHM due to more lattice-mismatching-induced defects and a stronger exciton−phonon coupling, respectively (Figures S3 and 4).

Therefore, the recombination and charge-transfer mechanisms can be described by the band diagram in Figure 3a to indicate how we manipulate the charge-transfer and recombination mechanisms. Upon photoexcitation, photoexcited carriers thermalize to the conduction band edge of the core, followed by either intrinsic exciton emission, or transfer to the Au nanoparticles, or transfer to the surface states by trap emission. Figure 3b shows that the ratio of the integrated PL intensity of trap emission (A_{trap}) and exciton emission (A_{exc}) initially decreases and then gradually increases with increase in temperature for both thickness shells, similar with the trend of the PL peak intensity ratio of I_{trap}/I_{exc} (Figure S5). This is due to the band offset reduction, since the band gap of CdSe increases with increase in temperature, which may correspond to the work function difference between the core and the shell.[32] The ratio of A_{trap}/A_{exc} can be described by a classic exponential relation with a tunneling rate

$$\sim \exp\left(-\alpha L\sqrt{KT}\right) \quad (1)$$

where L is the shell thickness, K is the Boltzmann constant, T is the temperature, and α is the fitting parameter. Assuming that the initial electron energy is close to zero due to band edge thermalization, for temperature region <320 K, both curves can be fitted by eq 1. The ratio of A_{trap}/A_{exc} for 6 ML sample exhibits a drastic drop (from 6.22 to 1.68), while a slight change (from 1.35 to 1.21) is present for the 12-ML sample, which reveals that the shell thickness has a dominant effect on the charge-transfer process compared to the temperature. For the temperature region >320 K, where the initial energy values dominate, both curves show increasing tendencies on a roughly same magnitude. It indicates that over the high-temperature region, the dominant effect on electron transfer is due to the change in temperature rather than shell thickness. This reveals that a higher temperature offers electron a larger thermal energy, facilitating photogenerated electron transfer to the shell surface irrespective of shell thickness.

2.2. Temperature-Dependent TRPL. The charge-transfer and recombination mechanisms indicated by Figure 3a are further qualitatively supported by the TRPL results using a biexponential or triexponential fitting for average lifetime for the main excitonic emission, as shown in Figures 4 and S6. Clearly, the earlier decay of CdSe/CdS/Au significantly reduces to less than 0.2 ns (faster than our instrument resolution of 0.2 ns) in contrast to the longer exciton lifetimes of the CdSe/CdS structures for both shell thickness structures.

The exciton lifetime τ can be described by the following relation

DOI: 10.1021/acsami.9b17339
ACS Appl. Mater. Interfaces 2019, 11, 48551−48555

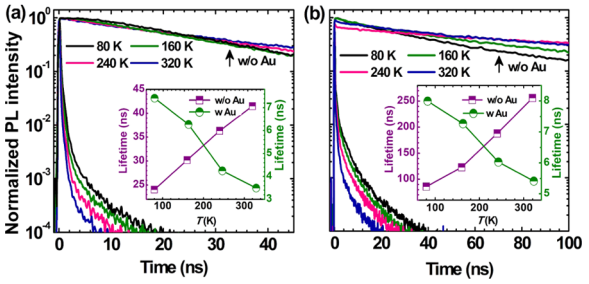

Figure 4. (a) Normalized temperature-dependent TRPL at the excitonic emission peak for the 6-ML shell CdSe/CdS without Au (abbreviated w/o Au) and CdSe/CdS/Au with Au (abbreviated w Au) in the temperature range from 80 to 320 K. (b) Same measurement for the 12-ML shell system. The insets show the corresponding average decay lifetimes for CdSe/CdS without Au or with Au.

$$\tau = \frac{1}{K_{rad}} + \frac{1}{K_{trap}} + \frac{1}{K_{Au}} \quad (2)$$

where K_{rad} is the radiative rate, K_{trap} is the charge-transfer rate to trap states, and K_{Au} is the transfer rate to Au. Therefore, the sharp decline of lifetime is due to the significant increase in charge-transfer rate because most photogenerated electrons are transferred to the nonradiative Au domain, resulting from the large driving force from the potential difference between the QD conduction band edge and Au Femi level. This is consistent with the ~2 order magnitude decrease in the exciton emission compared with that of the core/shell system, as shown in Figure S7. In particular, as shown in the insets of Figure 4 for CdSe/CdS QDs (without Au), the lifetime at an exitonic peak for both 6- and 12-ML shell CdSe/CdS QDs near-linearly increases with the increase in temperature from 80 to 320 K, which is consistent with the results of other groups.[25−27] A prolonged PL lifetime can be due to the decreased nonradiative recombination rate at a higher temperature.[32] Meanwhile, excitons of 12-ML shell QDs have a longer lifetime (85.88−255.97 ns) than that (24.0−41.49 ns) of 6-ML shell QDs over the temperature range. The highly increased lifetime in thicker-shell QDs (or called giant QDs) can be attributed to the reduced electron−hole spatial overlapping within the thicker shell, largely extending the recombination time between the electron and the hole.[33] Contrary to the increased exciton lifetime of CdSe/CdS with temperature, the lifetime of CdSe/CdS/Au exhibits a decreasing trend. This is most likely because, at higher temperatures, electrons with higher thermal energy would prefer to transfer to the Au region despite the shell thickness. As a result, the dominated transfer rate K_{Au} increases with increase in temperature and the overall exciton lifetime therefore decreases.

3. CONCLUSIONS

We manipulate the electron transfer to shell surface by varying the tunneling barrier height resulting from temperature variation and the tunneling barrier width resulting from shell thickness variation, which is demonstrated by an intrinsic exciton emission and trap emission in the near-infrared range. These charge-transfer and recombination mechanisms can be described by a tunneling model. Our study reveals a clear understanding of the charge-transfer mechanisms in a trap-related emission and provides a rational pathway of manipulating the electron tunneling with shell thickness and temperature in their photocatalysis and optoelectronics applications.

4. EXPERIMENTAL SECTION

4.1. QD Synthesis. CdSe/CdS core/shell QDs and CdSe/CdS/Au heterojunction QDs were synthesized using our previous procedure with minor modification.[2] The detailed synthetic condition is described in experimental details of the Supporting Information.

4.2. TEM Characterization. TEM measurements were carried on using a JEOL 2100F field emission transmission electron microscope at 200 kV. A toluene sample solution was drop-cast onto a TEM grid (300-mesh, copper) and dried at ambient conditions.

4.3. PL and TRPL Characterization. A iHR-550 spectrometer (HORIBA Scientific) was utilized for PL spectra measurement with a 450 W Xenon lamp as the excitation source in a FL-1039A illuminator box and symphony II CCD detector as the sensor for emission detection in accessible range from extended-UV to near-IR. TRPL spectra were measured on a FL3-22 spectrometer equipped with a picosecond photon detection module (TBX-05) and a 483 nm NanoLED-485L laser source controlled by a single photon counting controller (FluoroHub). Temperature-dependent PL and TRPL spectra were measured with participation of liquid nitrogen optical Cryostat (JANIS instrument) connected with a temperature controller Model-325. Each equilibration time is around 5 min after setting new temperature. For PL (TRPL) spectra measurement, all experimental parameters including excitation, integrate time, input or output slit, etc. (preset counts, pulse repetition rate, time range, etc.) are keep unchanged except for variable temperature.

■ ASSOCIATED CONTENT

Supporting Information

The Supporting Information is available free of charge at https://pubs.acs.org/doi/10.1021/acsami.9b17339.

Band gap and thermal activation energy calculation; absorption, emission spectra, and TEM image of CdSe/CdS QDs; emission spectra and TEM image of CdSe/CdS/Pt QDs; temperature dependence of FWHM and emission intensity; and fitting curves for emission decay process (PDF)

■ AUTHOR INFORMATION

Corresponding Authors

*E-mail: hsanabr@clemson.edu (H.S.).
*E-mail: ouchen@brown.edu (O.C.).
*E-mail: jianbogao.nano@gmail.com (J.G.).

ORCID

Exian Liu: 0000-0002-1031-7891
Hua Zhu: 0000-0003-2733-7837
Ying Shi: 0000-0002-6240-8795
Jianbing Zhang: 0000-0003-0642-3939
Apparao M. Rao: 0000-0002-1450-3499
Hugo Sanabria: 0000-0001-7068-6827
Ou Chen: 0000-0003-0551-090X
Jianbo Gao: 0000-0001-6203-5338

Notes

The authors declare no competing financial interest.

■ ACKNOWLEDGMENTS

We acknowledge funding from Clemson University. We are grateful to Russell Reynolds, Barrett Barker, and Michael Denz for their instrumental technical support. We thank the financial support from the program of China Scholarships Council

DOI: 10.1021/acsami.9b17339
ACS Appl. Mater. Interfaces 2019, 11, 48551−48555

(CSC). We also acknowledge Zehua Gao's technical support of QD synthesis and characterization.

REFERENCES

(1) Soni, U.; Tripathy, P.; Sapra, S. Photocatalysis from Fluorescence-Quenched CdSe/Au Nanoheterostructures: A Size-Dependent Study. *J. Phys. Chem. Lett.* **2014**, *5*, 1909−1916.
(2) Zhu, H.; Fan, Z.; Yu, L.; Wilson, M. A.; Nagaoka, Y.; Eggert, D.; Cao, C.; Liu, Y.; Wei, Z.; Wang, X.; He, J.; Zhao, J.; Li, R.; Wang, Z.; Grünwald, M.; Chen, O. Controlling Nanoparticle Orientations in the Self-Assembly of Patchy Quantum Dot-Gold Heterostructural Nanocrystals. *J. Am. Chem. Soc.* **2019**, *141*, 6013−6021.
(3) Zhu, H.; Nagaoka, Y.; Hills-Kimball, K.; Tan, R.; Yu, L.; Fang, Y.; Wang, K.; Li, R.; Wang, Z.; Chen, O. Pressure-Enabled Synthesis of Hetero-Dimers and Hetero-Rods through Intraparticle Coalescence and Interparticle Fusion of Quantum-Dot-Au Satellite Nanocrystals. *J. Am. Chem. Soc.* **2017**, *139*, 8408−8411.
(4) Ben-Shahar, Y.; Scotognella, F.; Kriegel, I.; Moretti, L.; Cerullo, G.; Rabani, E.; Banin, U. Optimal Metal Domain Size for Photocatalysis with Hybrid Semiconductor-Metal Nanorods. *Nat. Commun.* **2016**, *7*, No. 10413.
(5) Costi, R.; Saunders, A. E.; Elmalem, E.; Salant, A.; Banin, U. Visible Light-Induced Charge Retention and Photocatalysis with Hybrid CdSe-Au Nanodumbbells. *Nano Lett.* **2008**, *8*, 637−641.
(6) Haldar, K. K.; Sinha, G.; Lahtinen, J.; Patra, A. Hybrid Colloidal Au-CdSe Pentapod Heterostructures Synthesis and Their Photocatalytic Properties. *ACS Appl. Mater. Interfaces* **2012**, *4*, 6266−6272.
(7) Naskar, S.; Lübkemann, F.; Hamid, S.; Freytag, A.; Wolf, A.; Koch, J.; Ivanova, I.; Pfnür, H.; Dorfs, D.; Bahnemann, D. W.; Bigall, N. C. Synthesis of Ternary and Quaternary Au and Pt Decorated CdSe/CdS Heteronanoplatelets with Controllable Morphology. *Adv. Funct. Mater.* **2017**, *27*, No. 1604685.
(8) Li, Z.; Hu, Y.; Sun, Y. Promoting Photocatalytic Multiple-Electron Reduction in Aerobic Solutions Using Au-Tipped CdSe Nanorod Clusters. *Chem. Commun.* **2014**, *50*, 1411−1413.
(9) Dutta, S. K.; Mehetor, S. K.; Pradhan, N. Metal Semiconductor Heterostructures for Photocatalytic Conversion of Light Energy. *J. Phys. Chem. Lett.* **2015**, *6*, 936−944.
(10) Costi, R.; Saunders, A. E.; Banin, U. Colloidal Hybrid Nanostructures: A New Type of Functional Materials. *Angew. Chem., Int. Ed.* **2010**, *49*, 4878−4897.
(11) Ghosh, B.; Espinoza-González, R. Plasmonics for Improved Photovoltaic Devices. *JOJ Mater. Sci.* **2017**, *1*, No. 555558.
(12) Kim, M. R.; Xu, Z.; Chen, G.; Ma, D. Semiconductor and Metallic Core-Shell Nanostructures: Synthesis and Applications in Solar Cells and Catalysis. *Chem. - A Eur. J.* **2014**, *20*, 11256−11275.
(13) Alivisatos, A. P. Semiconductor Clusters, Nanocrystals, and Quantum Dots. *Science* **1996**, *271*, 933−937.
(14) Klimov, V. I.; Mikhailovsky, A. A.; Xu, S.; Malko, A.; Hollingsworth, J. A.; Leatherdale, C. A.; Eisler, H. J.; Bawendi, M. G. Optical Gain and Stimulated Emission in Nanocrystal Quantum Dots. *Science* **2000**, *290*, 314−317.
(15) Tisdale, W. A.; Williams, K. J.; Timp, B. A.; Norris, D. J.; Aydil, E. S.; Zhu, X. Y. Hot-electron transfer from semiconductor nanocrystals. *Science* **2010**, *328*, 1543−1547.
(16) Gao, J.; Kidon, L.; Rabani, E.; Alivisatos, A. P. Ultrahigh Hot Carrier Transient Photocurrent in Nanocrystal Arrays by Auger Recombination. *Nano Lett.* **2019**, *19*, 4804−4810.
(17) Cragg, G. E.; Efros, A. L. Suppression of Auger Processes in Confined Structures. *Nano Lett.* **2010**, *10*, 313−317.
(18) Chen, O.; Zhao, J.; Chauhan, V. P.; Cui, J.; Wong, C.; Harris, D. K.; Wei, H.; Han, H. S.; Fukumura, D.; Jain, R. K.; Bawendi, M. G. Compact High-Quality CdSe-CdS Core-Shell Nanocrystals with Narrow Emission Linewidths and Suppressed Blinking. *Nat. Mater.* **2013**, *12*, 445−451.
(19) Zhao, H.; Yin, H.; Liu, X.; Li, H.; Shi, Y.; Liu, C.; Jin, M.; Gao, J.; Luo, Y.; Ding, D. Pressure-Induced Tunable Electron Transfer and Auger Recombination Rates in CdSe/ZnS Quantum Dot-Anthraquinone Complexes. *J. Phys. Chem. Lett.* **2019**, *10*, 3064−3070.
(20) Zhu, H.; Yang, Y.; Wu, K.; Lian, T. Charge Transfer Dynamics from Photoexcited Semiconductor Quantum Dots. *Annu. Rev. Phys. Chem.* **2016**, *67*, 259−281.
(21) Tan, R.; Yuan, Y.; Nagaoka, Y.; Eggert, D.; Wang, X.; Thota, S.; Guo, P.; Yang, H.; Zhao, J.; Chen, O. Monodisperse Hexagonal Pyramidal and Bipyramidal Wurtzite CdSe-CdS Core-Shell Nanocrystals. *Chem. Mater.* **2017**, *29*, 4097−4108.
(22) Chauhan, H.; Kumar, Y.; Dana, J.; Satpati, B.; Ghosh, H. N.; Deka, S. Photoinduced Ultrafast Charge Separation in Colloidal 2-Dimensional CdSe/CdS-Au Hybrid Nanoplatelets and Corresponding Application in Photocatalysis. *Nanoscale* **2016**, *8*, 15802−15812.
(23) Wu, K.; Zhu, H.; Liu, Z.; Rodríguez-Córdoba, W.; Lian, T. Ultrafast Charge Separation and Long-Lived Charge Separated State in Photocatalytic CdS-Pt Nanorod Heterostructures. *J. Am. Chem. Soc.* **2012**, *134*, 10337−10340.
(24) Wu, K.; Rodríguez-Córdoba, W. E.; Yang, Y.; Lian, T. Plasmon-Induced Hot Electron Transfer from the Au Tip to CdS Rod in CdS-Au Nanoheterostructures. *Nano Lett.* **2013**, *13*, 5255−5263.
(25) Thuy, U. T. D.; Tu, L. A.; Loan, N. T.; Chi, T. T. K.; Liem, N. Q. Comparative Photoluminescence Properties of Type-I and Type-II CdTe/CdS Core/Shell Quantum Dots. *Opt. Mater.* **2016**, *53*, 34−38.
(26) Jing, P.; Zheng, J.; Ikezawa, M.; Liu, X.; Lv, S.; Kong, X.; Zhao, J.; Masumoto, Y. Temperature-Dependent Photoluminescence of CdSe-Core CdS/CdZnS/ZnS-Multishell Quantum Dots. *J. Phys. Chem. C* **2009**, *6*, 13545−13550.
(27) Rainò, G.; Stöferle, T.; Moreels, I.; Gomes, R.; Kamal, J. S.; Hens, Z.; Mahrt, R. F. Probing the Wave Function Delocalization in CdSe/CdS Dot-in-Rod Nanocrystals by Time-and Temperature-Resolved Spectroscopy. *ACS Nano* **2011**, *5*, 4031−4036.
(28) O'Donnell, K. P.; Chen, X. Temperature Dependence of Semiconductor Band Gaps. *Appl. Phys. Lett.* **1991**, *58*, 2924−2926.
(29) Valerini, D.; Cretí, A.; Lomascolo, M.; Manna, L.; Cingolani, R.; Anni, M. Temperature Dependence of the Photoluminescence Properties of Colloidal CdSeZnS Core/Shell Quantum Dots Embedded in a Polystyrene. *Phys. Rev. B* **2005**, *71*, No. 235409.
(30) Klimov, V.; Bolivar, P. H.; Kurz, H. Ultrafast Carrier Dynamics in Semiconductor Quantum Dots. *Phys. Rev. B: Condens. Matter Mater. Phys.* **1996**, *53*, 1463−1467.
(31) Laidler, K. J. The Development of the Arrhenius Equation. *J. Chem. Educ.* **1984**, *61*, 494−498.
(32) Balan, A. D.; Eshet, H.; Olshansky, J. H.; Lee, Y. V.; Rabani, E.; Alivisatos, A. P. Effect of Thermal Fluctuations on the Radiative Rate in Core/Shell Quantum Dots. *Nano Lett.* **2017**, *17*, 1629−1636.
(33) Selopal, G. S.; Zhao, H.; Tong, X.; Benetti, D.; Navarro-Pardo, F.; Zhou, Y.; Barba, D.; Vidal, F.; Wang, Z. M.; Rosei, F. Highly Stable Colloidal "Giant" Quantum Dots Sensitized Solar Cells. *Adv. Funct. Mater.* **2017**, *27*, No. 1701468.

DOI: 10.1021/acsami.9b17339
ACS Appl. Mater. Interfaces 2019, 11, 48551−48555